We are IntechOpen, the world's leading publisher of Open Access books Built by scientists, for scientists

6,900
Open access books available

186,000
International authors and editors

200M
Downloads

154
Countries delivered to

Our authors are among the

TOP 1%
most cited scientists

12.2%
Contributors from top 500 universities

CLARIVATE ANALYTICS
BOOK CITATION INDEX
INDEXED

WEB OF SCIENCE™

Selection of our books indexed in the Book Citation Index
in Web of Science™ Core Collection (BKCI)

Interested in publishing with us?
Contact book.department@intechopen.com

Numbers displayed above are based on latest data collected.
For more information visit www.intechopen.com

Interaction of Short Laser Pulses with Gases and Ionized Gases

Stephan Wieneke[1], Stephan Brückner[1] and Wolfgang Viöl[2]
[1] *Laser-Laboratorium Göttingen, Hans-Adolf-Krebs-Weg 1, 37077 Göttingen*
[2] *University of Applied Sciences and Arts, Von-Ossietzky-Str. 99, 37085 Göttingen*
Germany

1. Introduction

In this chapter, the interaction mechanisms between short laser pulses and gases, respectively pre-ionized gases are described in detail. Ordinarily, gases are transparent for electro-magnetic radiation. This is not valid any more when the intensity of radiation goes beyond a certain value. This barrier depends on the pressure, the gas type, the pulse length, the pulse repetition frequency, the beam diameter and the laser wavelength used. In order to understand the interaction mechanisms, knowledge about the propagation of electromagnetic radiation as well as knowledge about the absorption processes (for example: inverse bremsstrahlung) is necessary. Further, the mathematic models for the absorption processes and the following effects (as, for example, heating) of short laser pulses in gases and pre-ionized gases are explained. The appearing effects such as breakdown intensity or heating play an important role in the generation of new radiation sources. With specific laser pulses, individual radiation sources can be created (such as UV, EUV, soft X-ray).

2. Fundamentals of ionized gas generation

An ionized gas is called plasma to lay the focus on its consistence of electrified particles. This characteristic of plasma particles defines their major difference to a neutral gas. The most established way to generate a plasma is the electric gas discharge, for example in a spark or a flash of lighting. The ignition of an electric field occurs when a discharge between two electrodes starts to generate enough charge carriers to sustain itself. Due to the usage of an high performance laser, the so called laser induced plasmas can develop. For this, an intense laser pulse is focused on an existing target. The target is ionized this way; it is converted to plasma. To gain a laser induced plasma, solid targets, liquid targets or gas targets can be used. Because of their low vapor pressure, solid targets are particularly suitable for the use in vacuum. However it has to be ensured that a new area of the target will be hit with the laser pulse, for the material in the focal plane of the laser is destroyed during the plasma generation. The emission would be strongly decreasing after some pulses, because the laser would "drill" a hole in the material whereby no material would be left in the focus area (1). When the laser pulse meets the target, a shock wave is generated. This shock wave centrifuges particles out of the surface. Furthermore, particles are released because of thermal evaporation. A smaller amount of debris is generated when a liquid target or a gas target are used as medium. With liquid targets, particle densities similar to those in solid targets, can be reached (4; 5). The

liquid target is injected to the vacuum with the help of a nozzle assembly. The beam diameter here typically amounts to 10 - 30 μm, in which the liquid target is blasted with a pressure between 15 and 60 bar into the vacuum. Compared to solid targets, the debris appearing here during the plasma generation is smaller - about several orders of magnitude. In general it can be retained that a less debris is generated when smaller beam diameter is used. Ideally, the beam diameter has the size of the laser pulse focus diameter. Because the liquid target is made to follow up constantly through the nozzle assembly, it has to be removed from the vacuum system to perpetuate the vacuum conditions. Gas targets can be added intermittently through a valve. The laser pulses and gas shocks are synchronized so that the pulses are focused to a gas cloud. The disadvantage here lies in the fact that the density of gas has a lower value than the density of all-solids, so that an efficient absorption of laser beams is not possible.

2.1 Propagation of electromagnetic waves in a plasma

To understand the interaction between a plasma and laser beams, knowledge about the propagation electromagnetic waves in a plasma plays an important role. Here, a two liquid model can be used as a starting point for a precise analysis. Only the equation for the electrons are observed here, for the ions in a high frequency light source can be considered as immotile. For transversal verbs of small intensity, the current term is linearly simplified to $J = -e_0 n_e \bar{v}_e$ in the Maxwell-equations. All non-linear terms in order velocity moments can be neglected as well. The movement of the electrons in a plasma can be writen as (6):

$$m_e \frac{\partial \bar{v}_e}{\partial t} = -e_0 \vec{E}. \tag{1}$$

Using this equation, the following wave equation for electromagnetic waves in plasma arises from the Maxwell-equations:

$$\left(\frac{\partial^2}{\partial t^2} + \omega_p^2 - c_0^2 \nabla^2 \right) \vec{E} = 0. \tag{2}$$

The plasma frequency and the Debye length are important parameters of plasma. The plasma frequency describes the collective electron motion and equates to the natural frequency of electrons in a plasma. For a plane electromagnetic wave like $\vec{E} = E_0 e^{i(kx - \omega t)}$ the dispersion relation below is following up:

$$\omega^2 = \omega_p^2 + k^2 c_0^2. \tag{3}$$

It varies from the dispersion relation in vacuum in the summand ω_p^2. The most important interaction mechanism between plasma and laser field in of mild to moderate intensities (I $< 10^{15}$ W/cm^2 for 1 μm laser wave length) is the so called shock absorption. Again, the two liquids model offers a basis for a theoretical analysis if a shock term with the shock frequency between ions and electrons is included to the equation of motion for electrons: ν_{ei}.

$$m_e \frac{\partial \bar{v}_e}{\partial t} = -e_0 \vec{E} - m \nu_{ei} \bar{v}_e. \tag{4}$$

Thereby, a modified dispersion relation arises (for $\nu_{ei} << \omega$):

$$\omega^2 = \omega_p^2 + k^2 c_0^2 - i \omega_p^2 \frac{\nu_{ei}}{\omega^2}. \tag{5}$$

The real part matches with the solution without shocks. The negative imaginary part takes into consideration that the electromagnetic wave is damped during its dispersion in the

low-density plasma. In the process, the wave induces electron oscillations whose energy leads to an increase of the average electron energy because of the shocks of electrons with ions. Because of that, the electron temperature in the plasma is raised. Furthermore, higher ionization levels can be reached with the ions through shocks. This mechanism has a major importance for the generation of hot plasmas and is called *collisional absorption* or *inverse bremsstrahlung* according to the contrary process of bremsstrahlung, where kinetic electron energy is converted to radiation energy. In Figure 1 this process is shown schematically. A laser pulse meets a plasma with an electron density gradient. While the light wave passes the low-density plasma, it is damped and heats the plasma with the inverse bremsstrahlung. The wave is just able to spread up to the critical density in the plasma, there it is reflected. The area of the reflection point is the most effective are for an energy transfer from the radiation field to the plasma with the help of collisional absorption (7).
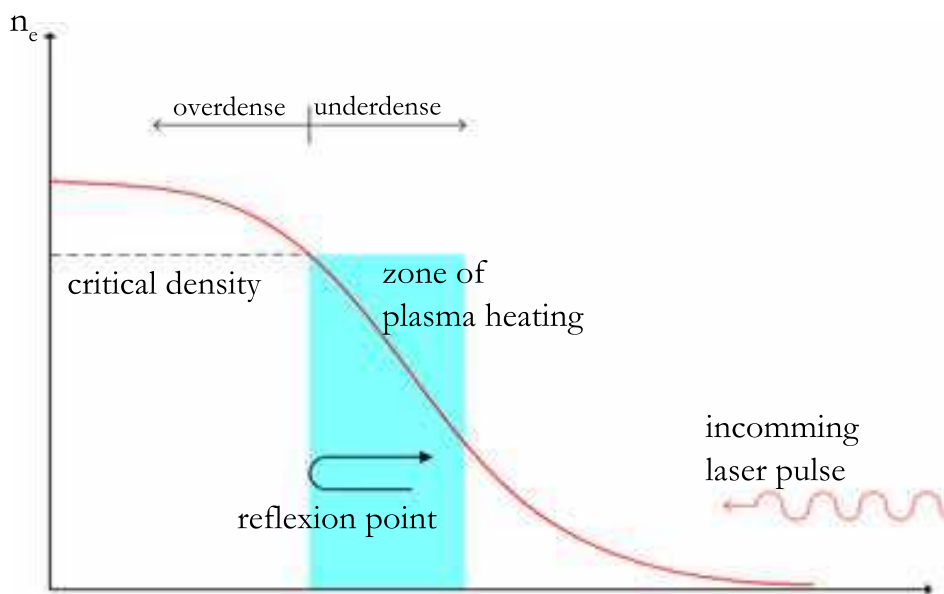

Fig. 1. One-dimensional illustration of the collisional absorption effect.

2.2 Collisional absorption - inverse bremsstrahlung

The absorption of laser radiation in a plasma, and thus the heating-up of the plasma, is affected by the inverse bremsstrahlung in the regime considered here. In this process a free electron accepts a radiation quantum of the laser beam. For reasons of the impulse conservation this is only possible in interaction with a neutral atom or an ion. The atoms or ions only absorb a small amount of the radiation energy and are primarily excited and heated indirectly by collisions with the accelerated electrons. While primarily neutral atoms exist at the beginning of the ignition, the electron-atom inverse bremsstrahlung dominates at that time. The according absorption coefficient α_{ea} is given as

$$\alpha_{ea} = \frac{1}{4\pi\epsilon_0} \cdot \frac{e^2 \nu_{ea} n_e \lambda_L^2}{\pi m_e c^3}. \tag{6}$$

Here n_e is the electron density, λ_L the laser wavelength and ν_{ea} is the impact frequency for impulse-exchanging collisions between electrons and neutral atoms. In an already ignited discharge, however, the electron-ion inverse bremsstrahlung plays the decisive role for the heating-up of the plasma. The absorption coefficient α_{ei} for electron-ion inverse bremsstrahlung applies to

$$\alpha_{ei} = \frac{n_e^2 e^6}{6\sqrt{3}n\epsilon_0^3 c\hbar\omega_L^3 m_e^2} \cdot \sqrt{\frac{m_e}{2\pi k_B T_e}} \cdot \left(1 - e^{-\frac{\hbar\omega_L}{k_B T_e}}\right)\bar{g}, \tag{7}$$

where ω_L is the laser frequency and n is the real part of the refractive index. The averaged Gaunt-factor $\bar{g}$, as adjustment to relativistic and quantum mechanical effects, applies to:
In this paper, the Nd:YAG laser is considered. In that case, a more precise expression for the Gaunt-factors can be written as:

$$\bar{g}_{Nd:YAG} = 6.2 \times 10^{-3}\left(\frac{T_e}{K}\right)^{0.42} + 0.86. \tag{8}$$

Figure 2 shows the linear absorption coefficient as a function of the plasma temperature for different electron densities n_e. These graphs clarify that, in order to achieve an effective absorption of laser radiation, the plasma requires a high electron density and a low electron temperature. Janulewicz *et al.* found that the absorption medium demands a concave electron density distribution with the maximum on the axis, against what the temperature distribution is to behave in reverse (2). This distribution is fulfilled in z-pinch plasmas and is experimentally determined in (3).
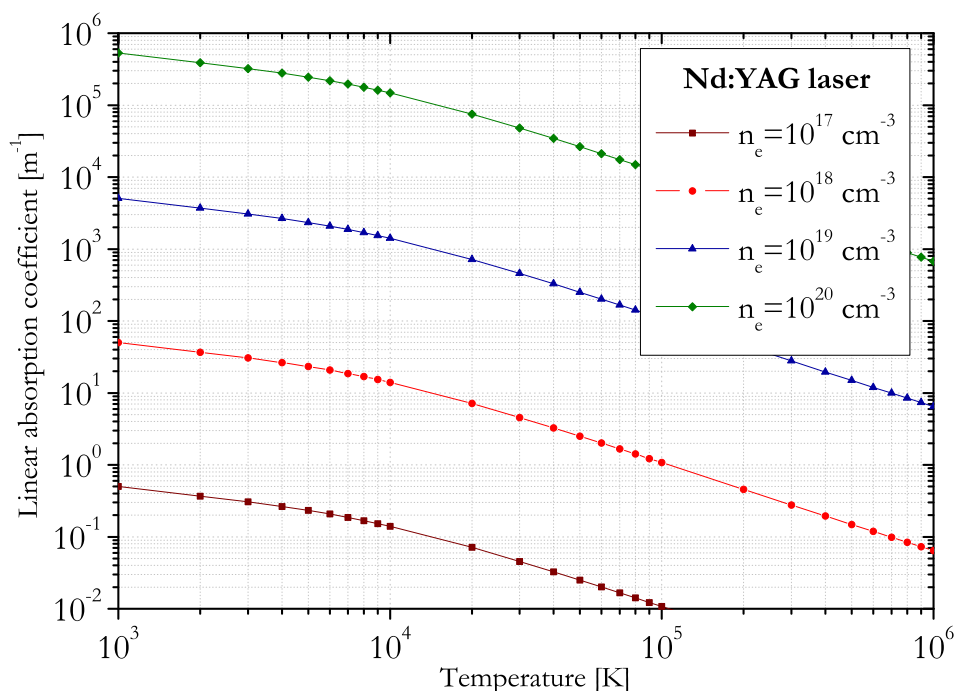

Fig. 2. Linear absorption coefficient as a function of temperature for varoius electron densities and for a wavelength of 1.06 μm.

2.3 Ignition behavior of laser based discharges

Ordinarily, gases are transparent for electromagnetic radiation. This does not apply any more when the radiation intensity exceeds a certain value, as it can happen in an high-energy laser. Just as it would happen in an ordinary discharge, the gas is ionized and the transmitted laser beam is damped. The minimal intensity needed to initiate a gas breakthrough can be found between $10^7 - 10^{11}$ W/cm^2. This threshold depends on the pressure, the gas type, the pulse length, the pulse repetition frequency, the beam diameter and the used wavelength. The

ionization can be effected by one or several of the following processes. If the field intensity is very high, the Columbo barrier is deformed and Tunnel ionization occurs. In the Tunnel ionization, electrons can be freed up the atom during one vibration of the electric field. In the multi photon ionization, an electron in the ground state is able to absorb several laser photons; it can be stimulated even beyond the ionization energy. This process is almost independent from the gas pressure. However, neither the Tunnel ionization nor the multi photon ionization plays a role when an Nd:YAG laser with its moderate field intensity and the small photon energy about 1.06 μm is used. The ionization is effected because of a cascade process; therefore, free electrons are needed. These electrons can be generated with multi photon ionization, cosmic radiation, a residual ionization accrued because of the high repetition rate of the laser pulses, or an electric discharge ignited before (9). Due to elastics shocks with neutral atoms, the electrons can absorb energy in the laser field and set free more electrons when they exceed the ionization energy with inelastic shocks with atoms or ions. These new electrons are integrated into the process as well. Referring to the cascade theory, the ignition intensity needed has a minimum at a certain pressure; it increases with the pressure. For the ignition intensity I_z in the focus of a laser needed to ignite a plasma in a gas, the following relation is given (8):

$$I_z \geq \frac{\epsilon_0 m_e c_0 E_I}{e_0^2 \ln 2} \cdot \frac{\omega_L^2 + \nu_{ea}^2}{\nu_{ea}} \cdot \left\{ \frac{1}{\tau_L} \cdot \ln\left(\frac{n_{eb}}{n_{e0}}\right) + \frac{D}{\Lambda_d^2} + h_a \nu_{ea} + \nu_{ve} + \nu_{vi} \right\}. \tag{9}$$

According to equation (9), the ignition threshold is proportional to the ionization energy E_I of the gas. The terms inside of the brackets do take various loss terms into consideration. They are described in the following passage (10): If the first term is dominant here because of a small laser pulse duration, it is called *time-determined* ignition. The ignition threshold is reciprocally proportional to the laser pulse duration τ_L and therefore defined through the whole energy flow. Here, n_{eb} is the electron density where the electron-ion bremsstrahlung is much more effective than the electron-atom bremsstrahlung. In the case under consideration, the ratio n_{eb}/n_{e0} accounts for 10^{13} (8). According to this model, a significant decrease of the ignition intensity needed because of the higher electron density n_{e0} at the beginning of the laser pulse can merely be expected in the case of a time-determined ignition. If the second term prevails (as, for example, in small pressures or focus volume) the ignition is called a *diffusion-determined* ignition. For the diffusion coefficient D it holds (8):

$$D = \frac{\langle v^2 \rangle}{3\nu_{ea}}. \tag{10}$$

Where the average quadratic speed $\langle v^2 \rangle$ of the electrons shall be such that the average electron energy corresponds with half of the ionization energy of gas:

$$\langle v^2 \rangle = \frac{2\langle E_e \rangle}{m_e} = \frac{E_I}{m_e}. \tag{11}$$

In case of a cylinder arrangement, the following equation is used for the diffusion length Λ_d (15):

$$\frac{1}{\Lambda_d^2} = \left(\frac{2,405}{R}\right)^2 + \left(\frac{\pi}{L}\right)^2. \tag{12}$$

R is taken as radius for the cylinder assumed here, L is its length. The equation (12) can be transcribed to a laser generated cylinder volume:

$$\frac{1}{\Lambda_d^2} = \left(\frac{2.405}{w_f}\right)^2 + \left(\frac{\pi}{2z_R}\right)^2 = \left(\frac{2.405}{w_f}\right)^2 + \left(\frac{\lambda_L}{2w_f^2}\right)^2. \tag{13}$$

Here, R is replaced by the radius of the laser beam waist w_f. The length L is replaced by the doubled Rayleigh lenght z_R in the discharge volume. If the ignition is diffusion-determined the ignition intensity scales with $1/w_f^2$. In the third term, charge carrier losses because of attachment are described. Due to the low xenon attachment coefficient h_a, this term can be neglected here. Losses based on elastic materials are described with the help of the fourth term. Here, $\langle E_e \rangle = E_I/2$ is assumed:

$$\nu_{ve} = \frac{2m_e \langle E_e \rangle \ln 2}{m_a E_I} \cdot \nu_{ea}. \tag{14}$$

The last term stands for the energy loss due to inelastic materials. It applies:

$$\nu_{vi} = \left(\tilde{\alpha} + \frac{\tilde{\beta}}{\Lambda_d^2}\right) \cdot \nu_{ea}. \tag{15}$$

This term is important for molecular gases, for they have a huge amount of excited states. For xenon, the material frequency $\nu_{ea} = 2 \cdot 10^8 \text{ s}^{-1} \cdot \text{p}$ can be presumed. Fig. 3 shows the behavior of the ignition intensity for xenon dependent from the pressure, for a Nd:YAG laser with a wavelength of $\lambda = 1.06$ μm. It is calculated with the help of equation (9). The experimentally achieved values according to (11), for a laser pulse duration about $\tau_L = 35$ ns as well as the experimentally achieved values following the work of (12) for a laser pulse duration of $\tau_L = 10$ ps were also simulated with this model. As a whole, an ignition intensity of 10^{16} W/cm^2 is calculated for xenon with a pressure of 13 Pa, an assumed beam focus of $2w_f = 50$ μm and a laser pulse duration of $\tau_L = 9$ ns. These experimental determined values accord with the simulated values very well. However we found out in the experiment that the gas ignition was not possible below a pressure og about 750 Pa.

3. Modelling of the interaction of laser puleses and neutral gases

3.1 Influence of the target density

To identify the influence of the target density on the achievable electron temperature, a laser pulse is coupled to a target at different target densities. The achievable maximum electron temperature is determinded numerically. As input parameter, a fit function of the experimentally determined laser pulse profile is used. With a repetition rate about 10 Hz, the laser system generates short NIR laser pulses with a maximum pulse energy about 750 mJ. The pulse width is ca. 9 ns in the FWHM. A lense with the focal width of $f = 150$ mm is used for the focusing of the laser pulse; it generates a focus diameter about 50 μm. The simulation results are shown in fig. 4. Here it is clearly to see that relevant electron temperatures cannot be generated with a laser pulse energy about 750 mJ in the relevant low pressure area about 10 Pa. This was already shown in the experiments in section 2.3. An operating pressure >1 kPa with a high initial particle density necessary to generate an adequate ionization and thereby electron temperature in a laser induced plasma. Because of that, liquid targets or solid targets are mostly used for laser induced plasmas. Another possibility to gain an efficient ionization with low operating pressure is the use of a stronger laser pulse. For an operating pressure of about 10 Pa, a laser pulse with the pulse energy of > 10 J is needed.
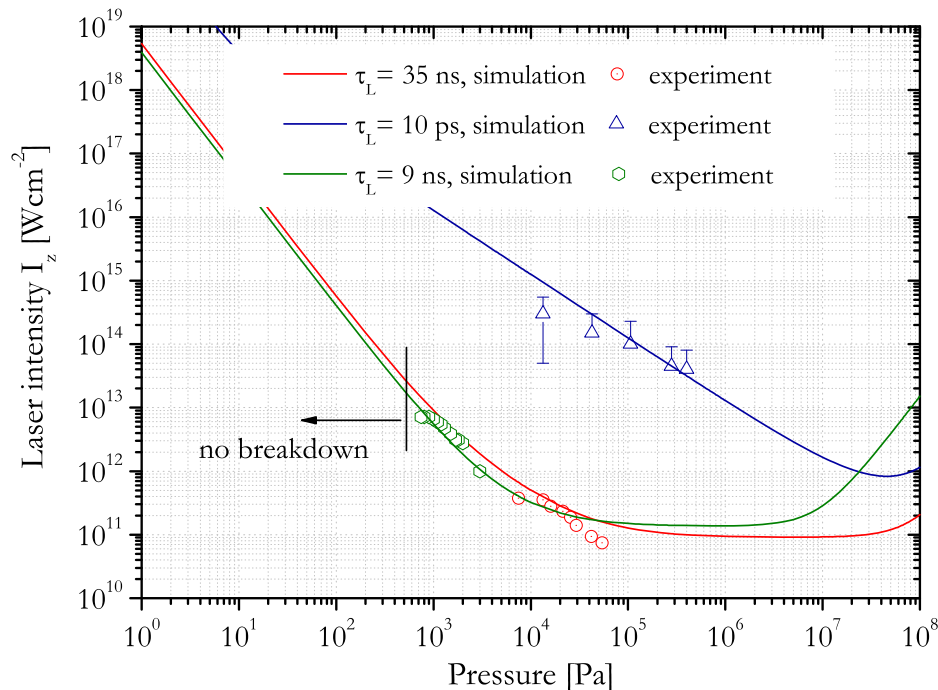
Fig. 3. Dependence of the breakdown intensity in addition to the pressure for different pulse duration times and a wavelength of 1.06 μm.

3.2 Influence of the laser pulse duration

The influence of the laser pulse duration on an efficient heating will be investigated in the following passage. As input parameter for the simulations a Gauss profile of the laser pulse is taken. Its width is varied between 0.5 - 30 ns. These simulations are carried out for different power densities (from 0.5 TW/cm^2 to 9.2 TW/cm^2). Here, the laser is coupled to a Xenon target at a gas density of 6 mg/cm^3. The fact that higher electron temperatures can initially be reached with increasing pulse rates (while the intensity stays the same) indicates a collisional absorption (inverse bremsstrahlung) as main mechanism for the plasma heating. The reason for this fact can be found through an observation of the electron density at the maximum electron temperature (red circles in figure 5).The most efficient plasma heating happens with a constant electron density at about $7\cdot10^{19}$cm^{-}3. This electron density is to find about one order of magnitude below the critical electron density of the laser wave length used. Above this electron density, the laser beam does not heat the plasma efficiently any more. With a growing laser intensity, this electron density of $7\cdot10^{19}$ cm^{-3} can be reached more quickly because of a higher target ionization. Supposedly, the optimal pulse duration postpones from a falling pulse intensity to shorter pulse durations.

3.3 Energy distribution and conversion efficiency

The time dependant behavior of the single shares of energy (kinetic energy, radiation energy, intern energy) of the plasma is important for an efficient change of the laser pulse to radiation energy of the plasma. A high amount of kinetic energy in the plasma leads to a high contamination rate of the components (debris), a high radiation component leads to a high conversion efficiency. For a better impact assessment, the different shares of energy for initial electron densities ne0 are calculated in a time-resolved manner. In fig 6 one can see the temporal relation of the energy distribution (radiation energy, kinetic energy and intern
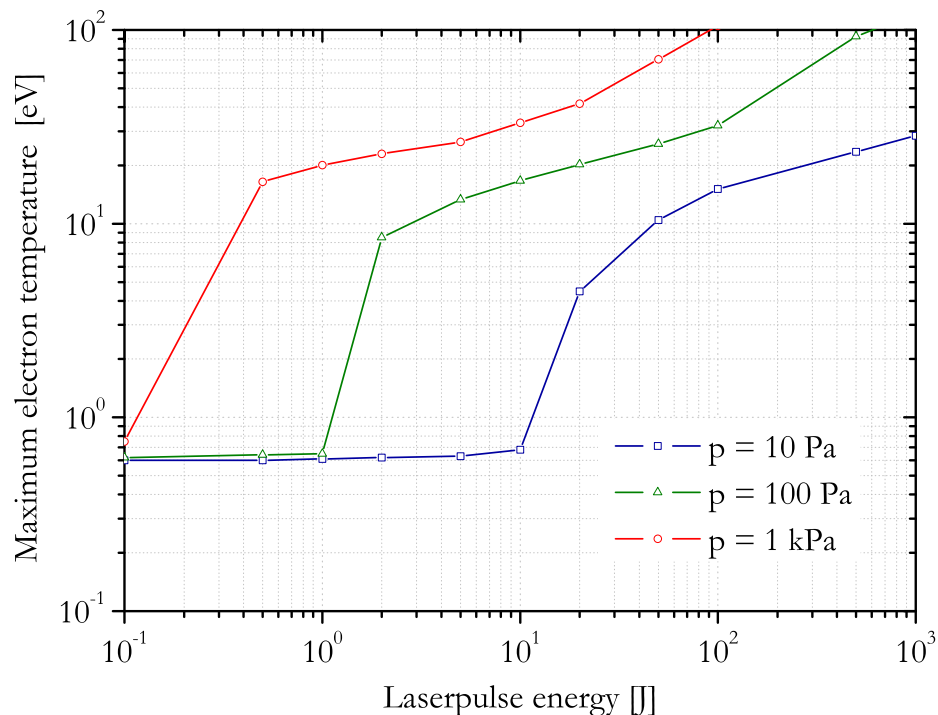
Fig. 4. Maximal reachable electron temperature in the plasma, dependent from the laser pulse energy for different pressures (target density).

energy in the plasma) for a xenon plasma heated with an Nd:YAG laser, E=1 J and 9 ns pulse duration, with an initial electron density of n_{e0}=10^{18} cm^{-3}. It is obvious that about 8 % of the laser pulse energy absorb by the plasma is emitted after 30 ns. In comparison, only 8 % are turned to kinetic energy and 4 % are turned to intern energy of the plasma (thermic + ionization-/ excitation energy). A huge part of the leftover intern energy is turned to kinetic energy, which means that the plasma is cooling down and expands. The same situation in shown in fig 7 for an initial electron density of 10^{19} cm^{-3}. Here, the attention is attracted to the fact that only 60 % are changed to radiation energy; therefore the kinetic energy increases to 17 % and the intern energy increases to 23 %. When the initial electron density is further increased, the radiation production decreases and the kinetic energy rises up until it reaches the critical density. However, if the initial electron density is reduced, the radiation production increases to a maximum, but the laser radiation is not completely coupled to the plasma. For a better description of this discovery, an absolute conversion efficiency is determined.

4. Modelling of the interaction of laser puleses and pre-ionized gases

In order to be able to provide information concerning the propagation of electromagnetic waves in a gas which is already ionized (pinch-plasma) and the heating connected to this, a modeling is done with Comsol Multiphysics. Here, the laser pulse is coupled to the face surface of a plasma assumed already generated. For the laser pulse, a Gauss profile is assumed. Fig. 8 shows a construction drawing and the model area. The laser pulse is focused to the electrically generated pinch-plasma through a lens. To facilitate the modeling, it is executed in the 2D axially symmetric mode.
In order to meet statements on the temperature field of a laser-intensified plasma, the knowledge of the spatial and temporal intensity $I(r,z,t)$ of the short laser pulse is necessary.
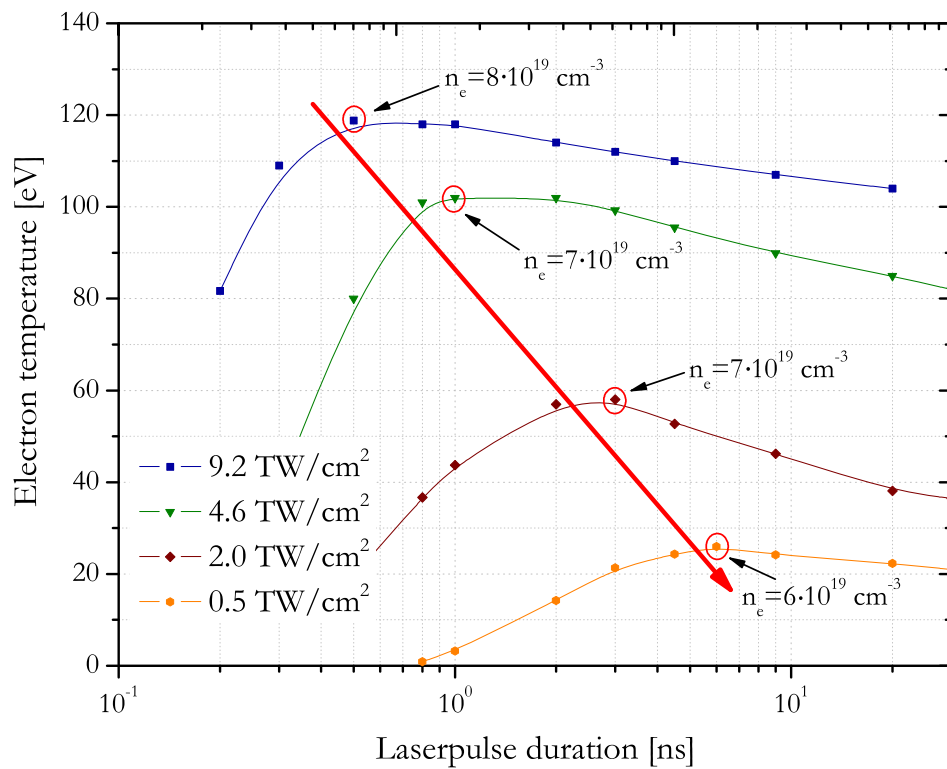
Fig. 5. Maximum reachable electron temperature of a laser induced xenon plasma (target density 6 mg/cm^3), dependent from the laser pulse duration for various laser intensities.

In vacuum, this distribution is given by

$$I(r,z,t) \quad = \quad \frac{I_0}{1+\left(\frac{z}{z_0}\right)^2} \exp\left(\frac{-2r^2}{w_f^2}\left(1+\left(\frac{z}{z_0}\right)^2\right)\right)$$

$$\cdot \exp\left(\frac{-4\ln(2)(t-\frac{z}{c_0})^2}{\tau_p^2}\right), \tag{16}$$

where I_0 is applied to:

$$I_0 = \frac{4\sqrt{\ln(2)}J_0}{\sqrt{\pi}\tau_p \pi w_f^2}. \tag{17}$$

The definition for the radius of the beam waist is

$$w_f = \frac{f\lambda_L}{w_0 \pi}. \tag{18}$$

Here f is the focal length of the optical system, w_0 is the $1/e^2$-beam radius at the lens, τ_p is the laser pulse duration, z_0 is the Rayleigh-length, J_0 is the energy of the laser pulse and z and r are the propagation directions, respectively. The propagation of an electromagnetic wave in a plasma is accompanied by its absorption in accordance with the Beer-Lambert law:
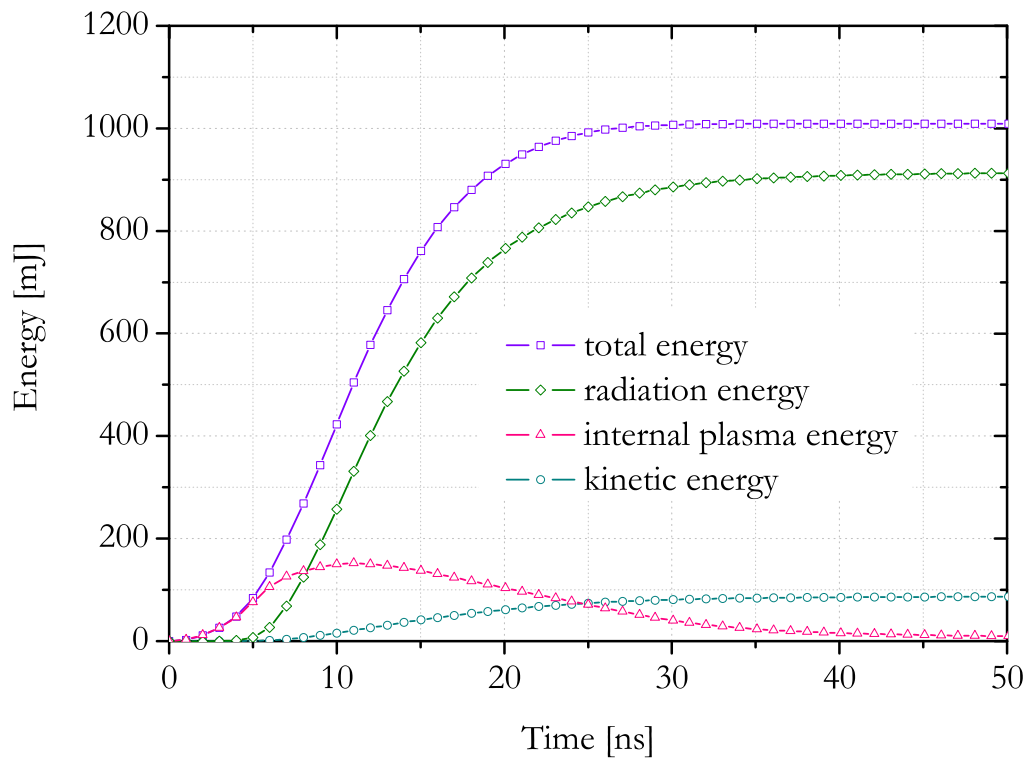
Fig. 6. Time dependency of the energy distribution of a xenon plasma, heated with a Nd-YAG laser pulse, with an initial electron density of $n_{e_0}=10^{18}$ cm^{-3}.

$$\ln\left(\frac{I_L(r,z,t)}{I(r,z,t)}\right) = -\int_0^z \alpha_{ei}dz, \tag{19}$$

where α_{ei} is the absorption coefficient and z is the length. The main mechanism of the absorption of probe radiation in the absence of absorption bands and lines is, as already mentioned in 2.2, the inverse bremsstrahlung. During the quick heating-up of the electrons, due to the laser pulse, no expansion work is achieved. The amount of heat dQ_L is supplied to the electrons per time unit. Standarized to the volume, with the absorption coefficient of the electrons for inverse bremsstrahlung α_{ei}, the heat source strength P_L results:

$$P_L(r,z,t) = \frac{1}{V}\frac{dQ_L}{dt} = \alpha_{ei}I_L(r,z,t). \tag{20}$$

The electron temperature changes agreeable to

$$\frac{dT_e}{dt} = \frac{2}{3n_ek_B}\alpha_{ei}I_L(r,z,t). \tag{21}$$

For the absorption coefficient α_{ei}, equation (7) is used. Because of the proportionality of the absorption coefficient to n_e^2, under certain circumstances, a possible rest ionisation from the previous laser pulse may play an important role. A high repetition rate and the effect of the magnetic field on the remaining ionisation can have a positive influence on the absorption of the plasma in this issue.

For the thermal conduction out of the central area of the discharge the continuity equation obtains:
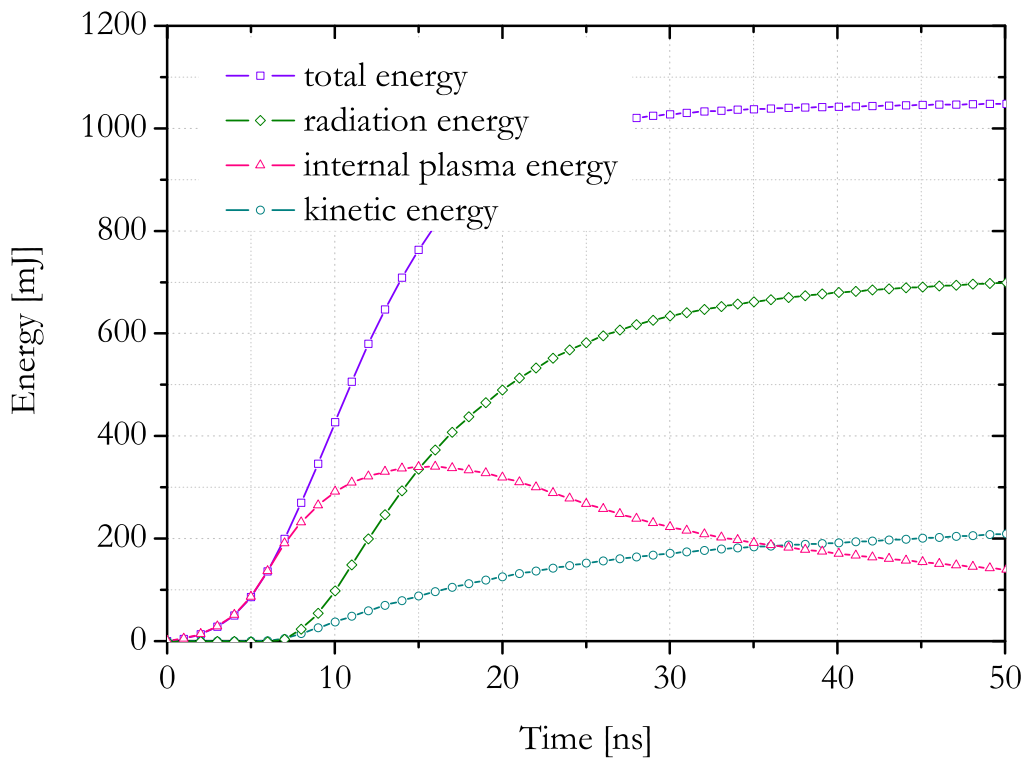
Fig. 7. Time dependency of the energy distribution of a xenon plasma, heated with a Nd-YAG laser pulse, with an initial electron density of n_{e_0}=10^{19} cm^{-3}.

$$\frac{dq}{dt} + \nabla \vec{j_w} = 0. \tag{22}$$

The heat flux obtains:

$$\vec{j_w} = -\kappa \nabla T_e, \tag{23}$$

where κ is the thermal conductivity. The temporal change of the electron temperature due to thermal conduction obtains:

$$\frac{dT_e}{dt} = \frac{2}{3n_e k_B} \nabla (\kappa \nabla T_e). \tag{24}$$

For the thermal conductivity, we use the expression

$$\kappa(T) = 4 \cdot 10^4 \left(9 - 8 \langle Z \rangle^{-\frac{1}{3}} \right) \left(\frac{T k_B}{e_0} \right)^{\frac{5}{2}} \frac{k_B}{e_0 \langle Z \rangle \ln \Lambda}. \tag{25}$$

Here e_0 ist the elementary charge of an electron. The term $\ln \Lambda$ describes the so-called Coulomb-logarithm, which applies to

$$\ln \Lambda = \ln \left[12\pi \left(\frac{\epsilon_0}{e_0} \right)^{3/2} n_e^{-1/2} T_e^{3/2} \right]. \tag{26}$$
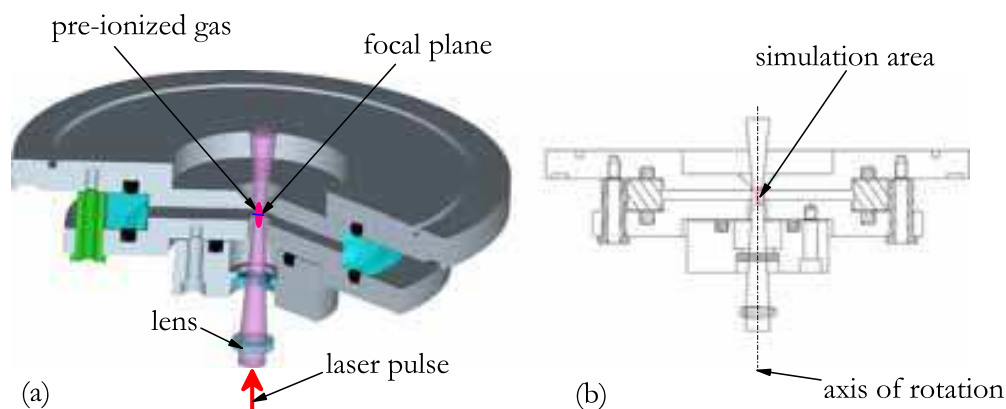
Fig. 8. (a) 3D scheme of the experimental setup. The laser pulse is focused onto the pre-ionized gas. (b) 2D scheme of the simulation setup. The red box shows the area modeled by the simulations.

4.1 Influence of the electron density

The coupling of laser beams and with that the heating of the plasma is strongly dependent from the absorption coefficient for inverse bremsstrahlung, i.e. from the electron density. The influence of the initial electron density on the reachable temperatures, respectively the propagation of laser radiation in the plasma is quantitatively simulated with the help of Comsol Multiphysics. Here, the laser pulse is coupled to the cross sectional area of the plasma cylinder with the help of a focusing optic. The focus diameter amounts 50 μm here. In this simulation, it is possible to give a constant, homogenous electron density to the plasma due to the smaller diameter of the laser beam in comparison with the pinch diameter. As an input parameter for the simulation, the initial electron density n_e is used. Fig. 9 shows the temporal and spacial temperature development in plasma at an initial electron density about 10^{17} cm^{-3}. Here one can see that the value chosen for the electron density is too small. The laser beam pervades the plasma almost unhampered (without absorption); only a small heating of the plasma occurs (about maximal 10 eV). With an increase of the initial electron density the absorption coefficient increases as well, so the laser beam can heat the plasma more efficiently. The maximum heating with the laser pulse is reached at an initial electron density of $n_e =$ $7 \cdot 10^{19}$ cm^{-3}. Fig. 10 shows that a laser beam can propagate exactly to its focal level, to the area of the highest intensity. Here, a local heating of the electrons up to 100 eV occurs. Another increase of the electron density, only an untimely absorption of the laser pulse would occur. This situation is shown in fig. 11 for an initial electron density of $n_e = 7 \cdot 10^{20}$ cm^{-3}. Here one can see that, due to the high electron density, the laser radiation is absorbed strongly from the dense plasma and cannot spread completely. The maximum temperature reached is generated far before the area with the highest power density (focal area).

Fig. 12 shows a quantitative diagram of the dependency of the electron temperature reached with different electron densities and laser pulses. It is obvious that the optimal heating can be reached with a plasma electron density of $^1/_{10}$ of the cut-off density of the particular laser wave length. This behavior was already found in section 3. If there is a higher electron density in the plasma, the laser beam cannot enter the plasma in an optimal way and thereby not heat it efficiently (16). As a result it can be said that knowledge concerning the occurring electron density in the plasma (development of free electrons thorough electric stimulation and the generation of free electrons with the laser pulse) is of major importance to gain an efficient plasma heating with a laser beam.
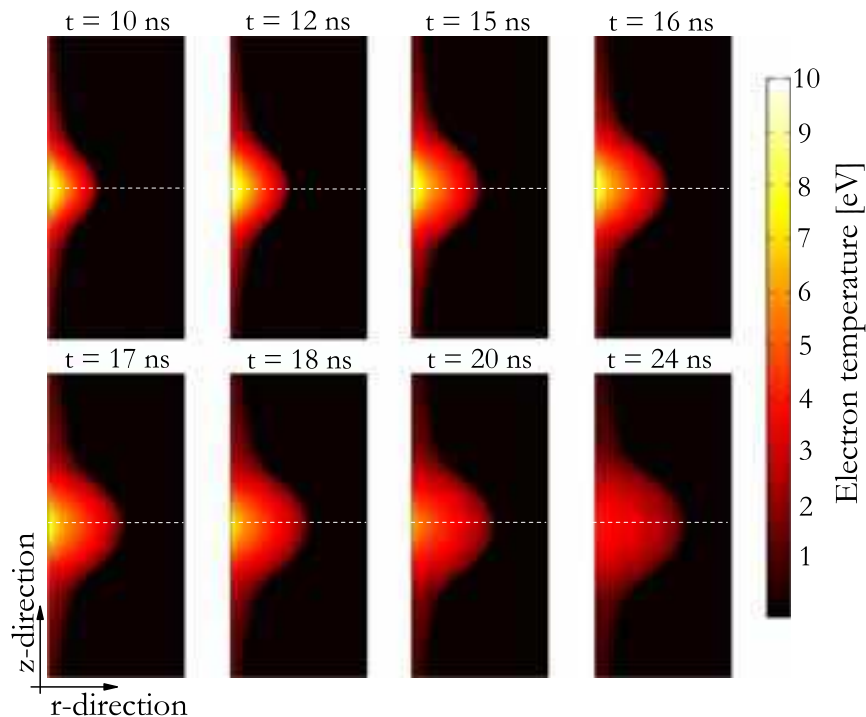
Fig. 9. Time development of the temperature distribution of a laser heated plasma with an initial electron density of $n_e = 10^{17}$ cm^{-3}. The interrupted line symbolizes the focal area. Here, a maximum electron temperature of about 10 eV is reached.

4.2 Influence of the distance of time between laser pulse and pinch-plasma

The distance of time between the generation of a pinch-plasma and the laser pulse plays a key role for an efficient combination of the two methods. Here, the basic differences for the result can be generated here. If on one hand the laser pulse is brought to the plasma exactly at the time of the pinch moment, the plasma is experiencing a further heating. On the other hand, the plasma can emit a double pulse generated in the extreme ultraviolett spectrum (EUV) when the laser pulse is timely staggered with the pinch moment. These guesses are to be examined with the help of simulations. For HELIOS-CR has only limited possibilities to simulate laser and pinch-plasma combination, some simplifications and assumptions are to be made. The basic idea is it to describe the pinch plasma as a pre-pulse with a defined energy. This pre-pulse is used o generate the plasma. The main pulse (laser pulse), timely staggered, is used to heat the plasma. The plasma expands isotherm during the radiation process and adiabatic without radiation, which means that it is possible to influence the density profile and the temperature of the plasma with a timing of the pre-pulse and the main pulse and phase them to the highest conversion efficiency for the desired wavelength. The pinch-plasma is described as a pre-pulse with a duration about 10 ns (time duration of the pinch) and an energy of 600 mJ as Gau intensity profile. The main pulse follows after a variable temporal shift with a pulse duration of 9 ns and an energy of 750 mJ. Figure 13 shows the temporal development of electron density temperature and density for three different, timely staggered laser pulses. In the figures 13a and 13d, the laser pulse follows the pinch moment with about 100 ns. Here, the plasma is not heated to a point above the temperature generated by the pinch-plasma (maximal 19 eV) because the plasma did already cool down after about 20-30 ns. However the laser pulse causes another plasma heating up to 16 eV. This way, two sequenced
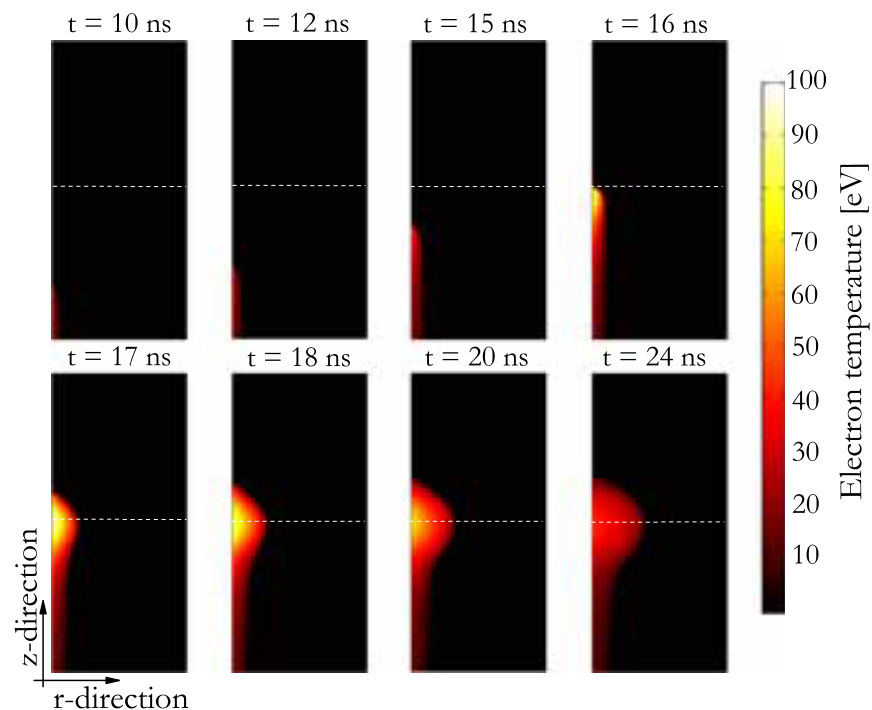
Fig. 10. Time development of the temperature distribution of a laser heated plasma with an initial electron density of $n_e=7 \cdot 10^{19}$ cm^{-3}. The interrupted line symbolizes the focal area. Here, a maximum electron temperature of about 100 eV is reached.

radiation pulses in the extreme ultraviolet spectral range can be generated. In the figures 13c and 13f, the laser pulse is coupled to the plasma simultaneous to the pinch moment. This generates a further plasma heating. The maximum temperature that can be reached is about 38 eV for this special case. These results do point out the importance of the time difference Δt between the pinch moment and the laser pulse coupling. On the one hand, a further plasma heating is possible, and on the other hand, two two sequenced radiation pulses in the extreme ultraviolet spectral range can be generated.

5. Experimental investigation

For all experimental investigation methods, an active mode locked Nd:YAG laser with two additional amplifier stages is used. It generates pulses with a half-width about 9 ns at maximal 0.8 J pulse energy. The laser runs at a maximum repetition frequency of 10 Hz, or it operates with single pulses. For the experiments, the pinch plasma has a voltage about 7 kV. The total capacity is about 46 nF at a total inductivity of 9.2 nH. The total energy of the hollow cathode triggered Z-pinch adds up to 1.1 J. Fig 14 shows a scheme of the experimental setup for a synchronization of the laser pulse and the hollow cathode triggered Z-pinch discharge. Due to the unsteady ignitions of the Z-pinch discharges, some measures for a synchronization of the laser pulse with the hollow cathode triggered Z-pinch discharges are necessary. The additional laser pulse heating of the plasma needs a fast reproducible laser triggering with a close relation to the pinch moment. To hit the plasma in a compacted state (durability about 10 ns) with the laser, a sufficiently strong and jitter free trigger signal is necessary about 100 ns before the main discharge occurs. For the avalanche breakdown of the hollow cathode triggered Z-pinch has a huge jitter of 50 μs, the laser pulse timing cannot be carried
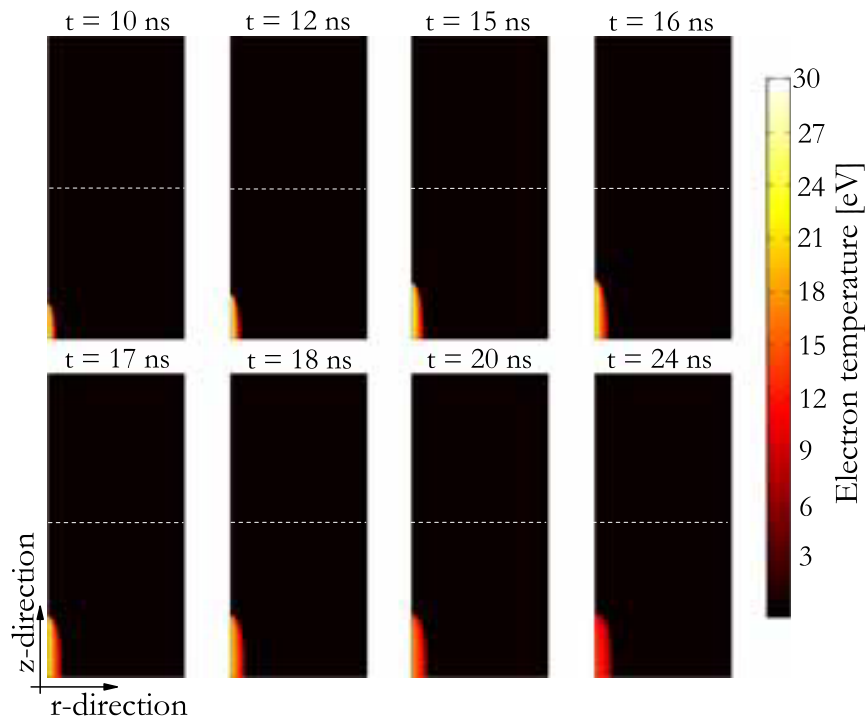
Fig. 11. Time development of the temperature distribution of a laser heated plasma with an initial electron density of $n_e=10^{20}$ cm^{-3}. The interrupted line symbolizes the focal area. Here, a maximum electron temperature of about 30 eV is reached.

out with the 4-Channel Delay-Generator. The trigger event has to emerge from discharge course to be hit. The trigger signal cannot be generated by the control elements of the hollow cathode triggered Z-pinch because of the unavoidable delay caused by the 4-Channel Delay Generator, some meters of coaxial cable and the laser electronics itself. Through, one of the hollow cathode discharge characteristics modeled (13) and experimentally approved (14) is the fact that it emits an intense electron beam shortly before the avalanche breakdown occurs. Because of that, a Faraday cup is used in the experiment to collect the discharges. It is added close to the anode bore. The electric potential of the Faraday cup becomes negative because of the appearance of the intense electron beam. When a high-impedance resistor (ordinarily 10^9 - 10^{11} Ω) is used, a measurable voltage increases. This voltage gives a sufficient signal about 100-200 ns [1] before the main discharge occurs, with a jitter about maximal 5 ns.

5.1 Laser-induced re-heating of pre-ionized gases

Figure 15 shows the experimentally determined xenon spectra with and without laser pulse heating. The laser pulse is coupled to the plasma about 90 ns after the avalanche breakdown. The spectra show that the spectrum intensity duplicates, but no new lines are generated with the laser pulse heating. The reason for this is that the pinch-plasma did already cool down because of the expansion. It seems that the laser pulse can only effect another plasma heating. According to this, two hot plasmas with a time delay ($\Delta t \approx$ 90 ns) and almost similar electron temperature and radiation power emerge. Due to the exposure time of the CCD camera (t=20 ms), two radiation events are integrated to the extreme ultraviolet spectral range; with that a higher intensity can be reached. This behavior of the timely delayed laser plasma

---

[1]dependent from the gas used: N_2, O_2, Xe, Ar, CO_2
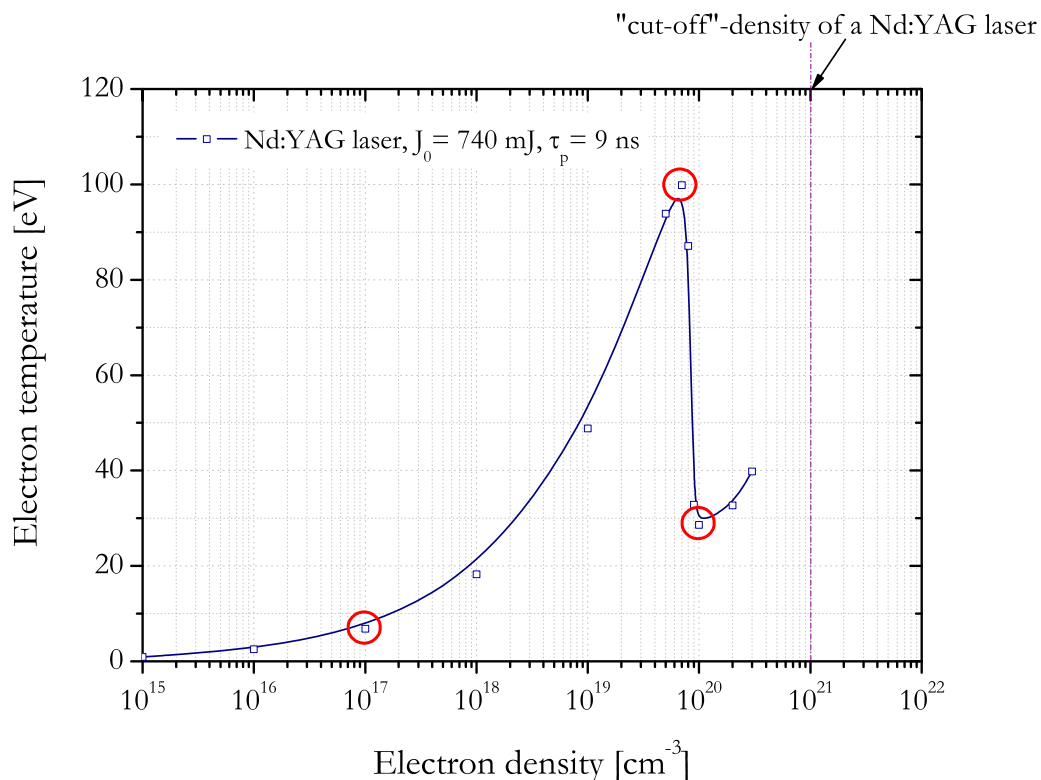
Fig. 12. Development of the electron temperature in plasma, dependent from the electron density during the plasma heating with the Nd-YAG laser pulse. The red circles show the values simulated in Fig. 9 - 11.

coupling was already simulated in section 4.2. The timely delayed EUV radiation pulses can be used as starting points for new application fields, such as, for example, the "pump and probe methods". Figure 15 shows the experimentally determined extreme ultraviolet spectra of a xenon z-pinch plasma combined with a short laser pulse. The time difference between the z-pinch plasma (in pinched state) and the incident laser pulse is about 100 ns. As a consquence the laser does not hit the plasma at peak compression but rather the residuals of the discharge. As shown the intensity over the whole spectral range increases at about a factor of two compared to the sole z-pinch plasma, whereas the sole laser without a discharge has no effect (green line). The spectra are taken from a single shot each. A comparison of the spectral line intensities of each spectra, as shown in (16), leads to an estimated electron temperature of $T_e \approx 70$ eV in both cases.

5.2 Laser-induced additional heating of pre-ionized gases

Figure 16 shows an experimentally determined spectrum order. Here, the pinch-plasma is run at a repetition rate of 1 Hz and one spectrum is taken, respectively. After 20 pulses, a laser pulse is additionally coupled to the plasma (20 pulses). The timely delay between avalanche breakdown and laser pulse here indeed only amounts to about 10-20 ns. The figure shows that the additional plasma heating occurs as desired. Furthermore one can see that not every laser pulse causes an additional plasma heating because of timely instabilities of the laser pulses. The newly generated spectral lines do mostly derive from helium-like nitrogen-ions. The strongest lines in the 1s3d and 1s4d change-over at 17.3865 nm and 13.0286 nm. A comparison

of the intensity ratio of the lines from different ionization stage with simulated spectra gives an electron temperature about 57 eV in the plasma. When this temperature is reached, the intensity of the emitting line in the water window at 2.786 nm is about 50 times higher than the strongest line at 16.255 nm. This shows that it was possible to generate an efficient emitter in the area of the water window.

6. References

[1] Rolf, F. (2005). Entwicklung eines Rastermikroskopes für den Einsatz an Laborquellen im EUV Spektralbereich, *Phd Thesis, Bayerische Julius-Maximilians-Universität Würzburg*, 2005

[2] Janulewicz, K. A. (2004). Review of state-of-the-art and output characteristics of table-top soft x-ray lasers, *X-Ray Spectrom.*, Vol. 33, No. 4, 2004, 262-266

[3] Brückner, S. and Wieneke, S. and Viöl, W. (2008). Theoretical and experimental investigations of the suitability of low-current z-pinch plasma as an absorption medium for laser radiation, *Contrib. Plasma Phys.*, Vol. 48, No. 8, 2008, 577-585

[4] Rymell, L. and Hertz, H. M. (1993). Droplet target for low-debris laser-plasma soft X-ray generation, *Opt. Commun.*, Vol. 103, No. 105, 1993, 110

[5] Richardson, M. and Torres, D. and Depriest, C. and Jin, F. and Shimkaveg, G. (1998). Mass-limited, debris-free laser-plasma EUV source, *Opt. Commun.*, Vol. 145, No 109, 1998, 112

[6] Attwood, D. T. (2000), *Soft X-rays and Extreme Ultraviolet Radiation - Principles and Applications*, Cambridge University Press

[7] Vogt, U. (2002). Röntgenemission aus laserinduzierten Plasmen: Einfluss von Laserintensität und Pulsdauer bei verschiedenen Targetsystemen, *Phd Thesis, Fakultät Mathematik und Naturwissenschaften der Technischen Universität Berlin*, 2002

[8] Chan, C. H. (1973). Significant loss mechanismus in gas breakdown at 10.6 μm, *J. Appl. Phys.*, Vol. 44, No. 3, 1973, 1179-1188

[9] Viöl, W. (1988). Hochleistungs-CO_2-Laserpulse hoher Repetitionsfrequenz zur Erzeugung optischer Entladungen, *Phd Thesis, Mathematisch-Naturwissenschaftliche Fakultät der Universität Düsseldorf*, 1988

[10] Burger, M. (2003). Spektroskopische Untersuchung und Modellierung eines lasererzeugten Heliumplasmas im starken Magnetfeld, *Phd Thesis, Matematisch-Naturwissenschaftliche Fakultät der Heinrich-Heine-Universität Düsseldorf*, 2003

[11] Bergqvist, T. and Kleman, B. (1966). Breakdown in gases by 1.06 μm laser radiation, *Ark. Fys.*, Vol. 31, No. 2, 1966, 177-189

[12] R. K. Avery (1984). Interpretation of picosecond laser-induced breakdown in argon and xenon, *J. Phys. D: Appl. Phys.*, Vol. 17, 1984, 1657-1663

[13] Boeuf, J.P. and Pitchford, L.C. (1991). Pseudospark discharges via computer simulation, *IEEE Trans. Plasma Sci.*, Vol. 19, No. 2, 1991, 286-296

[14] Benker, W. and Christiansen, J. and Frank, K. and Gundel, H. and Hartmann, W. and Redel, T. and Stetter, M. (1989). Generation of intense pulsed electron beams by the pseudospark discharge. *IEEE Trans. Plasma Sci.*, Vol. 17, No. 5, 1989, 754-757

[15] Raizer, Y. P. (1997). Breakdown of Gases in Fields of Various Frequency Ranges, In: *Gas Discharge Physics*, Springer-Verlag, Berlin

[16] Wieneke, S. and Brückner, S. and Viöl, W. (2008). Simulating the heating of z-pinch plasmas with short laser pulses, *Journal of Plasma Physics*, Vol. 74, No. 3, 2008, 361-369
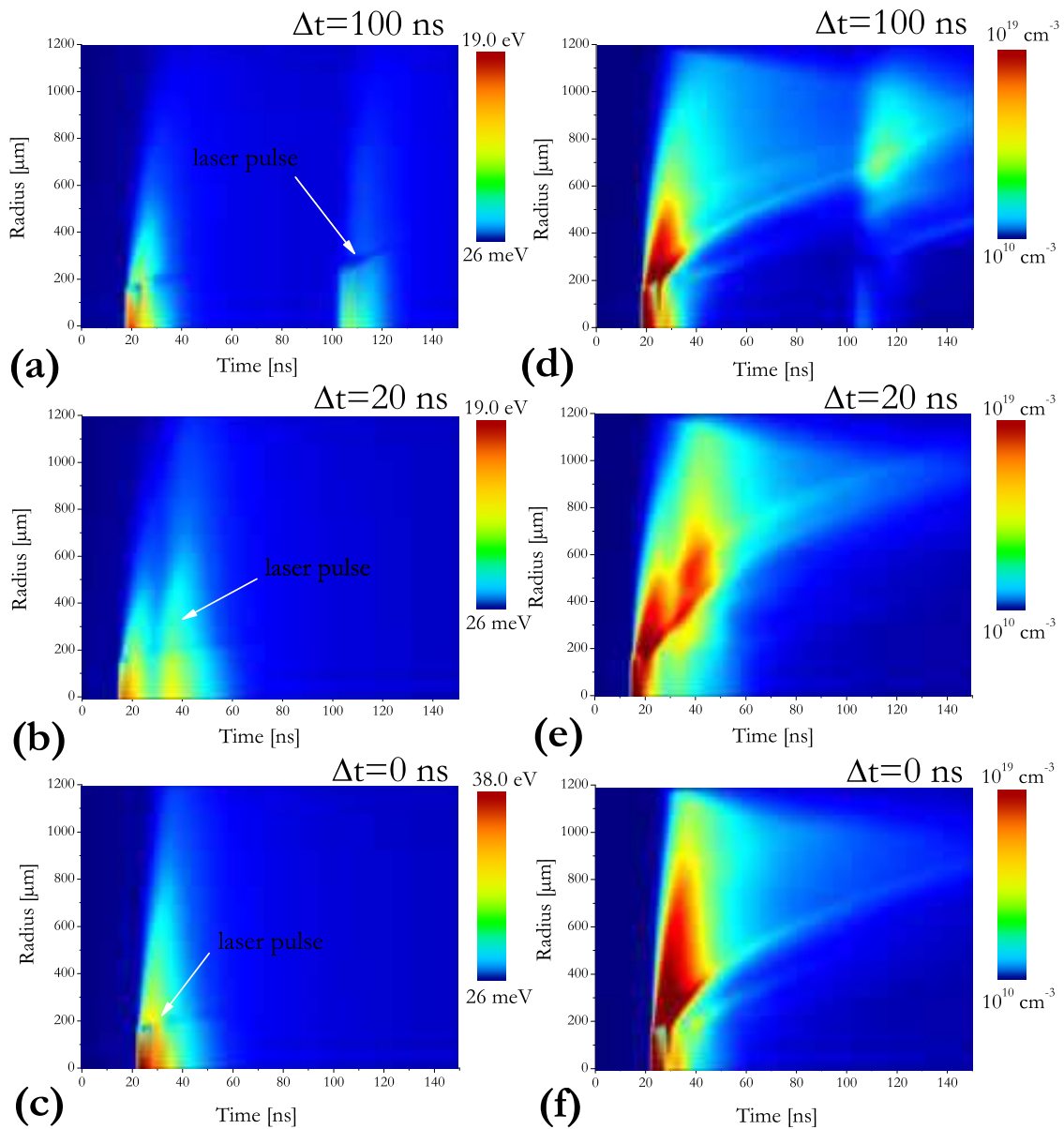
Fig. 13. Simulated time dependence of a laser heated xenon pinch plasma for different delay times of the laser pulse for the electron temperature (a-c) and electron density (d-f).
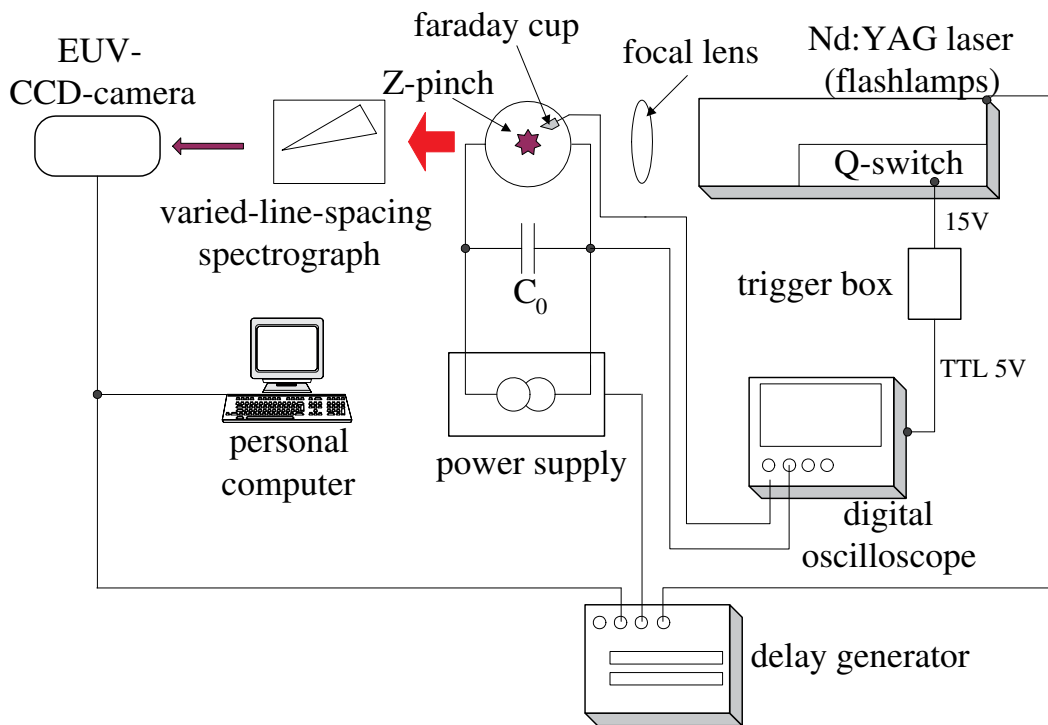
Fig. 14. Experimental setup for a synchronization of the Z-pinch discharge and the laser pulse
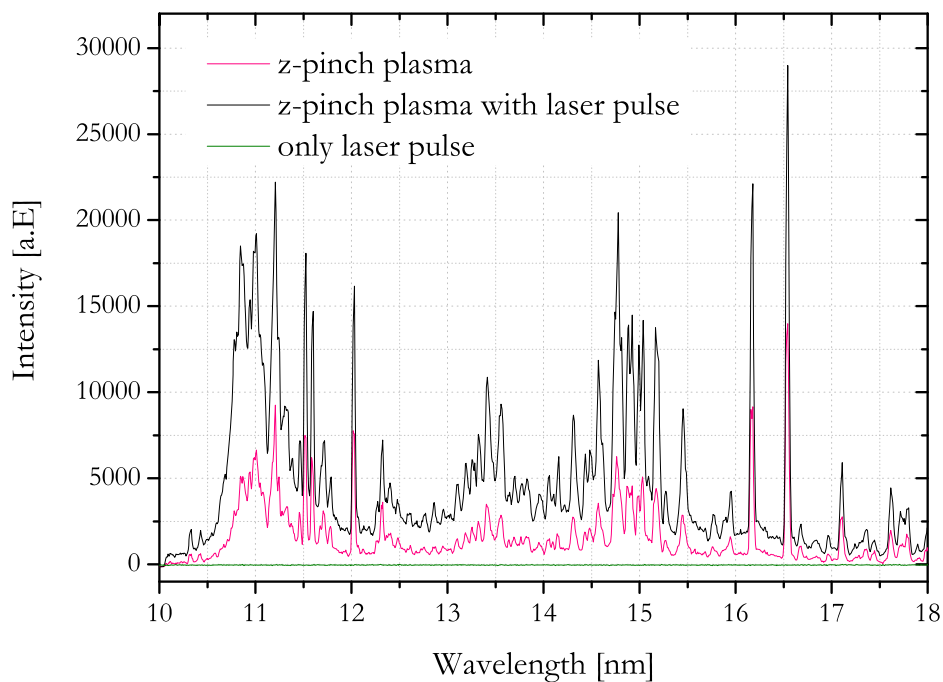
Fig. 15. Experimentally determained EUV spectra of a xenon z-pinch plasma (black) and a combined laser pulse reheated z-pinch plasma (red). In comparison the sole laser pulse does not create any EUV radiation, because the charge carrier density is to low for the breakdown of the discharge (green).
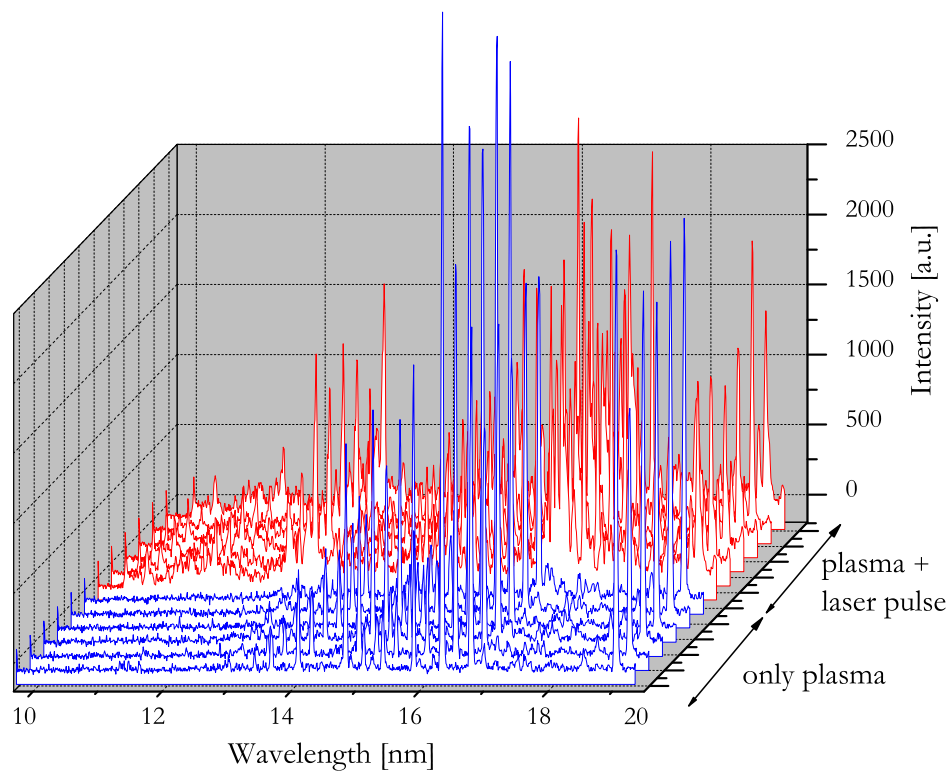
Fig. 16. Experimentally determined emission spectra of a nitrogen plasma with and without laser pulse heating. The spectra are continuously gathered at a repetition rate about 1 Hz (20 pulses are taken with and without laser pulse, respectively). The charging voltage is about 7 kV at a gas pressure about 6 Pa.
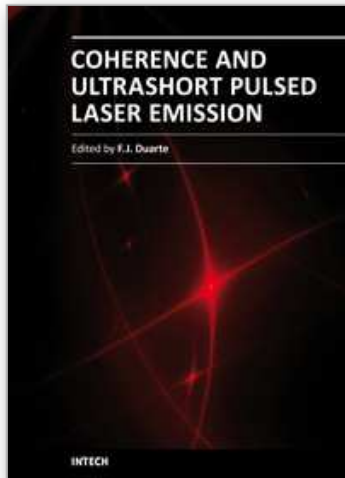
Coherence and Ultrashort Pulse Laser Emission

Edited by Dr. F. J. Duarte

In this volume, recent contributions on coherence provide a useful perspective on the diversity of various coherent sources of emission and coherent related phenomena of current interest. These papers provide a preamble for a larger collection of contributions on ultrashort pulse laser generation and ultrashort pulse laser phenomena. Papers on ultrashort pulse phenomena include works on few cycle pulses, high-power generation, propagation in various media, to various applications of current interest. Undoubtedly, Coherence and Ultrashort Pulse Emission offers a rich and practical perspective on this rapidly evolving field.

How to reference

In order to correctly reference this scholarly work, feel free to copy and paste the following:

Stephan Brückner, Wolfgang Viöl and Stephan Wieneke (2010). Interaction of Short Laser Pulses with Gases and Ionized Gases, Coherence and Ultrashort Pulse Laser Emission, Dr. F. J. Duarte (Ed.), ISBN: 978-953-307-242-5, InTech, Available from: http://www.intechopen.com/books/coherence-and-ultrashort-pulse-laser-emission/interaction-of-short-laser-pulses-with-gases-and-ionized-gases

INTECH

open science | open minds